Nanoscale

Supporting Information

Tailoring Morphological and Chemical Contributions of Nanoscale Charge Transfer for Enhanced Triboelectric Nanogenerators

Received 00th January 20xx,
Accepted 00th January 20xx

DOI: 10.1039/x0xx00000x

Jong Hun Kim[a#], Da Woon Jin[a#], Jae Hyeon Jeon[a], Dheeraj Kumar[a], HongYeon Yoon[b], Hunyoung Cho[b], Hyotcherl Ihee[b,c], Jeong Young Park[b] and Jong Hoon Jung[a]**

[a]Department of Physics, Inha University, Incheon 22212, Republic of Korea

[b]Department of Chemistry, Korea Advanced Institute of Science and Technology (KAIST), Daejeon 34141, Republic of Korea

[c]Center for Advanced Reaction Dynamics (CARD), Institute for Basic Science (IBS), Daejeon 34141, Republic of Korea

[#] These authors contributed equally.

*Corresponding authors: jeongypark@kaist.ac.kr and jhjung@inha.ac.kr

Sample preparation and device characterization

PDMS films were fabricated using conventional spin-coating and curing methods. The PDMS elastomer and cross-linker (Merck KGaA, Korea) were completely mixed at three different weight ratios, ranging from 5:1 to 10:1, and followed by degassing under vacuum for 30 min. A certain amount of the resulting PDMS mixture was dropped onto Si-substrate and spin-coated at 500 rpm for 30 sec. Then, it was transferred to ITO-coated polyethylene terephthalate (PET) substrates and cured on a hot-plate at 80 °C for 2 hours. The effective surface area of the PDMS was 1 cm×1 cm, and it was 310 μm thick (Fig. S1), regardless of the chemical ratio. To deliver a mechanical perturbation, we used a custom-made device capable of applying a periodic compressive force to TENG device using a linear motor. The amplitude of tapping force and frequency were set at 30 N and 1 Hz, respectively, throughout the measurement. The output current signal was acquired by ultra-low noise current amplifier. All electrical measurements were conducted in a Faraday cage to minimize noise. Since the active area of capacitance is ultimately determined by the smallest among the two metal electrodes and the middle dielectric, the upper ITO, being smaller than the others, was used to estimate the charge density.

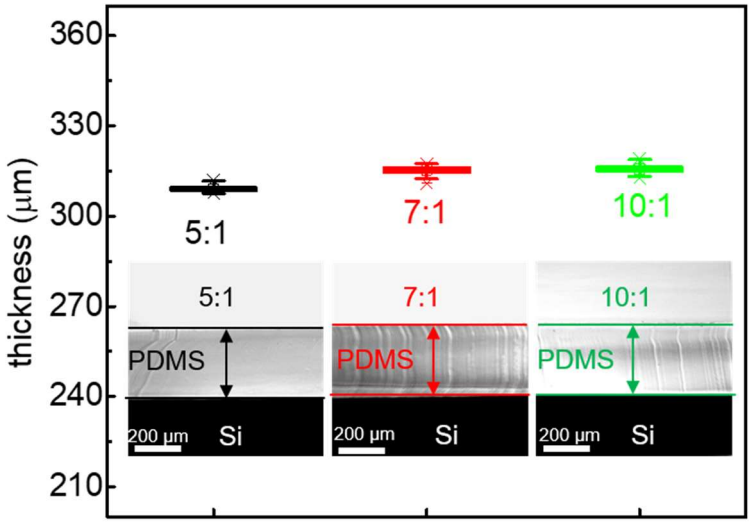

Fig. S1 The boxplots that present the thickness distribution of three different kinds of Si-supported PDMS: the inset shows optical microscope images corresponding to (left) 5:1, (middle) 7:1, and (right) 10:1, respectively. The average thickness of three samples was measured to be ~309, ~315, and ~316, for 5:1-, 7:1-, and 10:1-PDMS, respectively. The thickness deviation among the three samples is at most ~2 %.

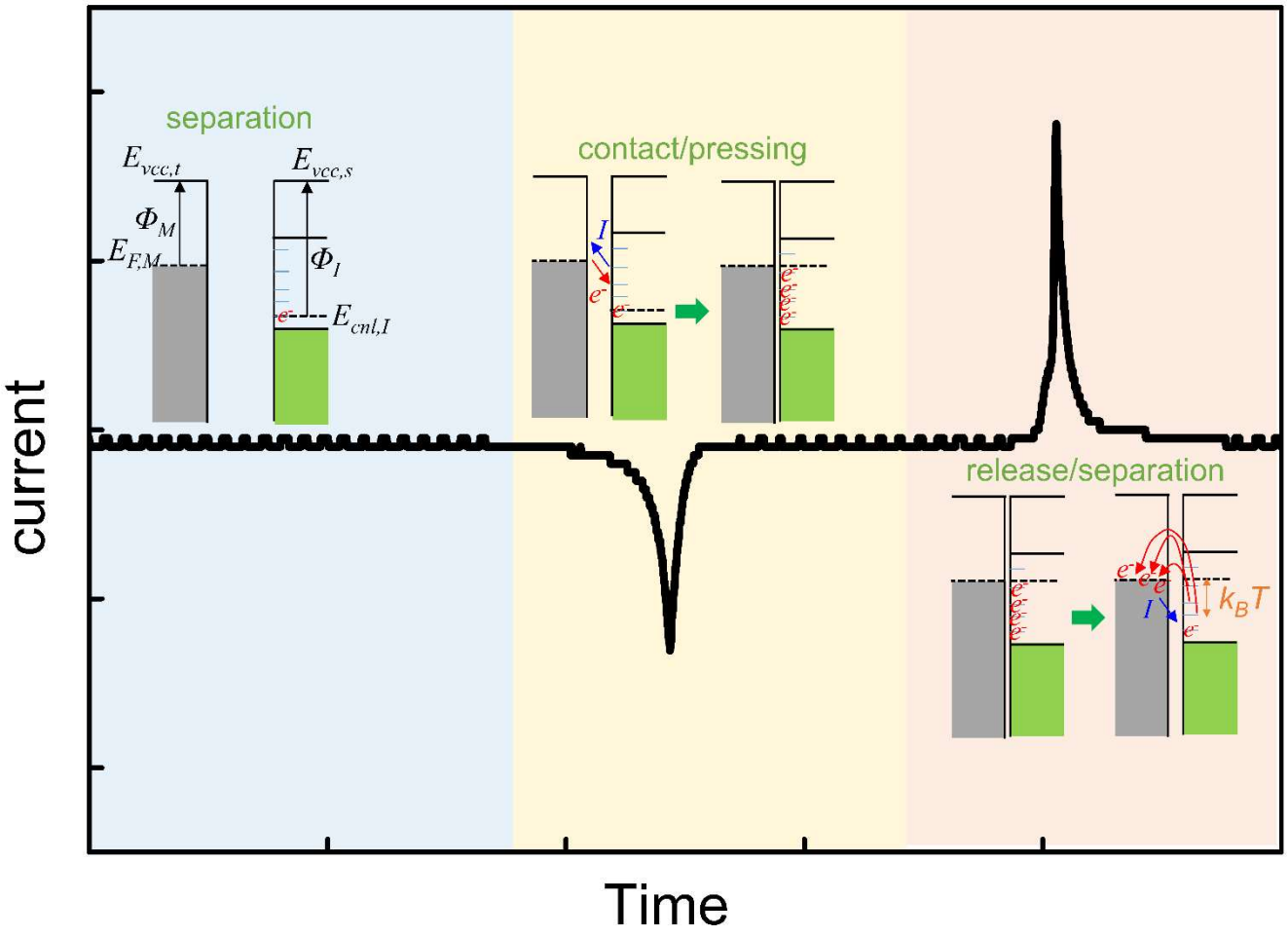

Fig. S2 The typical current output of a TENG based on a pairing of ITO and PDMS. (inset) Schematic diagrams of the charge generation and transfer mechanisms corresponding to the current output. Since electrons in the surface states of the two contact materials are exchanged and reconfigured during the contact/pressure, a negative pulse is generated. This, in turn, induces a charge flow equal to the number of exchanged carriers from the external circuit via electrostatic induction. The charge flow can be reversed when the contacting materials are released/separated. As the two contact materials are separated, the displaced charges attempt to return to their original states, assisted by thermal energy, resulting in the opposite charge flow via the external circuit. [1-3]

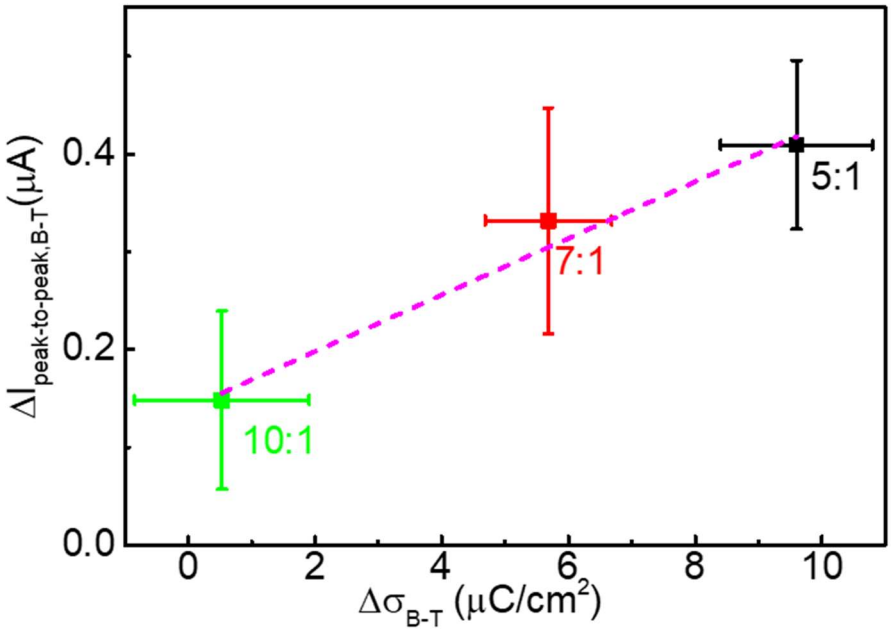

Fig. S3 The correlation between charge density difference, $\Delta\sigma_{B\text{-}T}$ and the peak-to-peak current difference, $\Delta I_{peak\text{-}to\text{-}peak,B\text{-}T}$ between the top side and the bottom side.

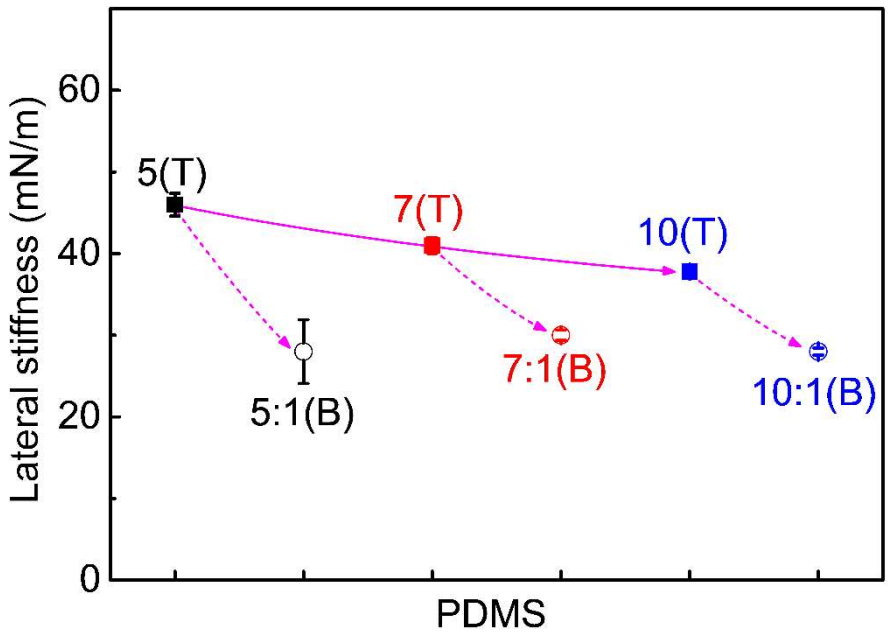

Fig. S4 The total lateral stiffness (k_{tot}) depending on PDMS types. k_{tot} is simply estimated from the edge slope of LFM loop in Fig. 2(b).

The measured total lateral stiffness (k_{tol}) is given as[4, 5]

$$\frac{1}{k_{tot}} = \frac{1}{k_{cant}} + \frac{1}{k_{cont}} \qquad \text{(S1)}$$

where k_{cant}, and k_{cont} are the lateral stiffness of cantilever and tip-sample contact, respectively.

Also, the contact stiffness can be represented as:

$$\frac{1}{k_{cont}} = \frac{2-\nu_{tip}}{8rG_{tip}} + \frac{2-\nu_{sample}}{8rG_{sample}} \qquad \text{(S2)}$$

where ν, G, and r represent the Poisson ratio, shear modulus, contact radius, respectively. Since both the cantilever stiffness, and the shear modulus of silicon tip are much higher[4, 6] than those of polymers, [7], the measured slope is primarily associated with the weakest bonding made between the tip and polymer sample. Therefore, the measured lateral stiffness is approximated to that of sample itself.

$$k_{tot} \propto \frac{8rG_{sample}}{2-\nu_{sample}} \qquad \text{(S3)}$$

Therefore, the reduced slope means the decrease of modulus in the bottom-side-PDMSs.

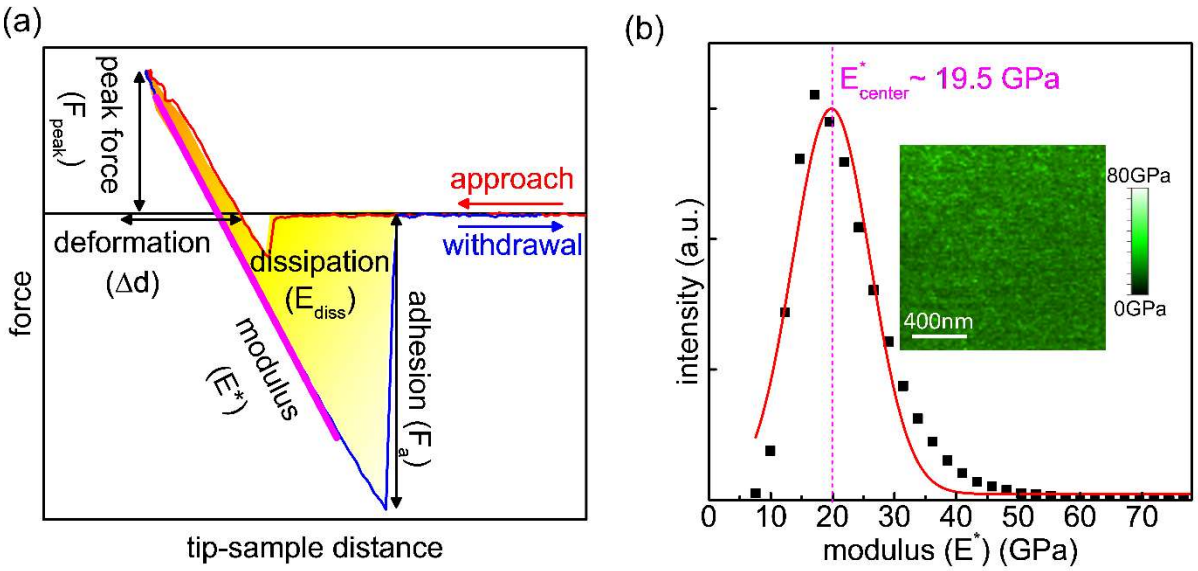

Fig. S5 (a) Schematic of force-distance curve under PF-AFM. It illustrates the definition of modulus, adhesion, deformation, and energy dissipation. (b) The distribution of reduced modulus (E*) on 300 nm-thick SiO_2-substrate. Gaussian fitting (red line) was performed for calibrating the tip radius: (inset) the extracted modulus images of SiO_2.

In our study, all the PF-AFM data were acquired at the peak force of 50 nN, and Z-piezo travel distance of 130 nm. The scan rate is set at 0.5 Hz. The elastic constant of tip was calibrated based on the thermal tune method, as mentioned in LFM. As shown in Fig. S5, the adhesion force is defined as the maximum force to pull the tip off from the surface. The energy dissipation (E_{diss}) and the deformation (Δd) are defined as the area encompassed by the loading and unloading curves and the distance between the contact point and the turn-away point, respectively.

Assuming a modified Herzian model,[8] reduced modulus (E*) can be estimated from the slope of unloading curve using the following equation:

$$E^* = \frac{3}{4}\frac{(F_L - F_a)}{\sqrt{R \cdot \Delta d^3}} \qquad \text{(S4)}$$

where R, Δd, F_L, and F_a are the tip radius, deformation, loading force, and adhesion force, respectively. From the measured E* values, the sample modulus can be extracted by using the following equation:

$$\frac{1}{E^*} = \frac{1-\upsilon_s^2}{E_s} + \frac{1-\upsilon_t^2}{E_t} \qquad \text{(S5)}$$

where E_s (E_t) and v_s (v_t) are the elastic modulus and the Poisson's ratio of the sample (tip), respectively. Using the equation of S4 with S5, the tip radius, R was calibrated as ~ 4 nm by measuring the modulus of SiO_2 substrate (E_s = 72 GPa).[9, 10] It was assumed that both v_s and v_t are 0.3.

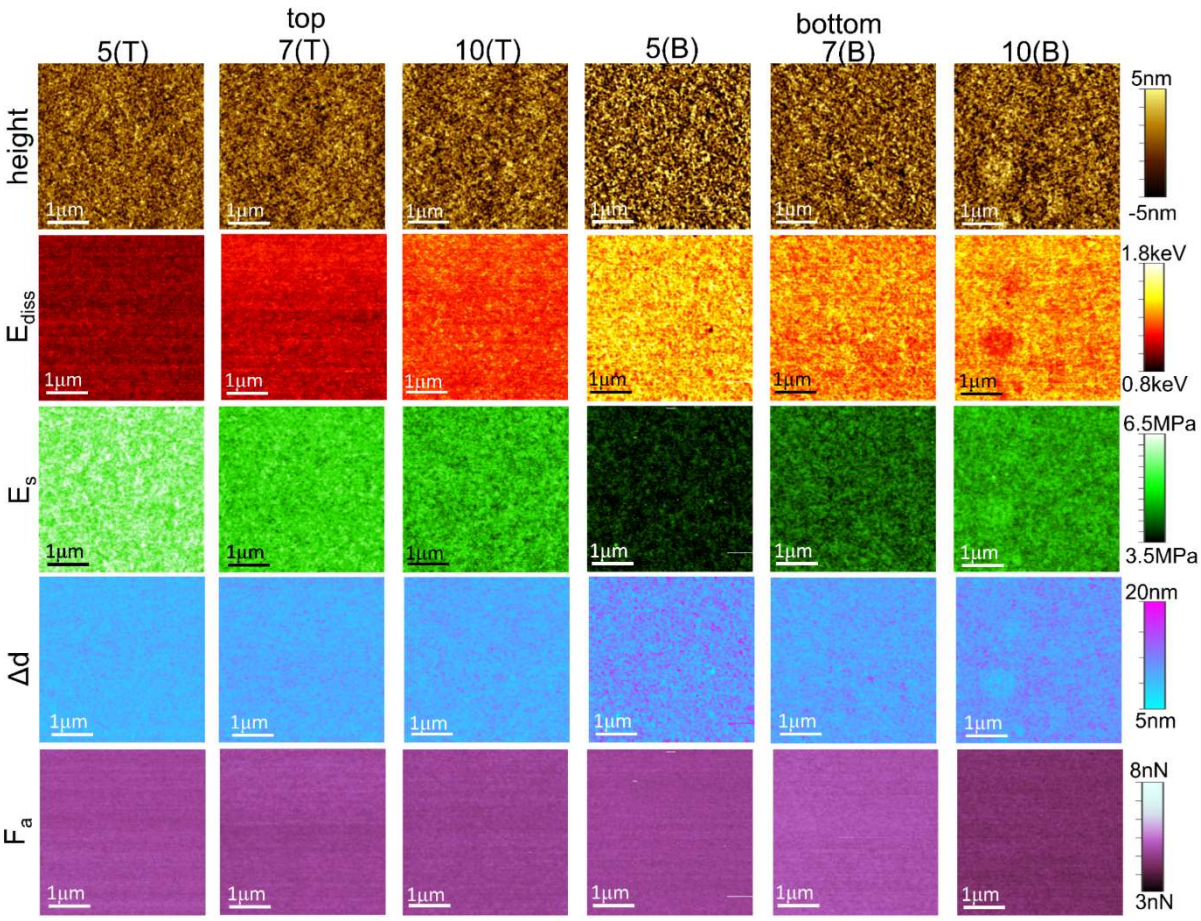

Fig. S6 PF-AFM images for 6 different types of PDMS. (row 1) topography, (row 2) energy dissipation, (row 3) modulus, (row 4) deformation images of PDMS. The images in each column were simultaneously taken. Note that a common intensity scale was used for each signal channel.

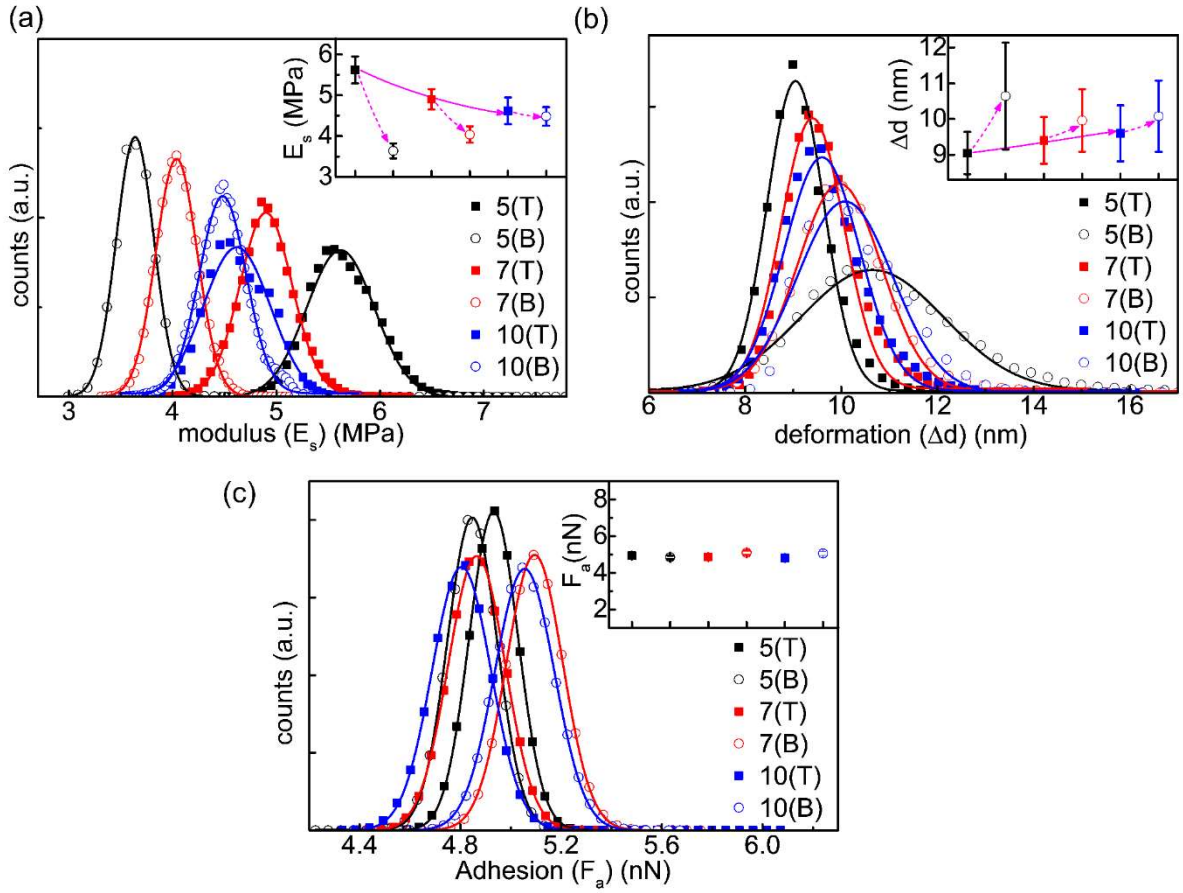

Fig. S7. Distributions of (a) modulus, (b) deformation, and (c) adhesion obtained from Fig. S6. Gaussian fitting lines were overlaid on the data points, from which the Gaussian center values were individually plotted in each inset.

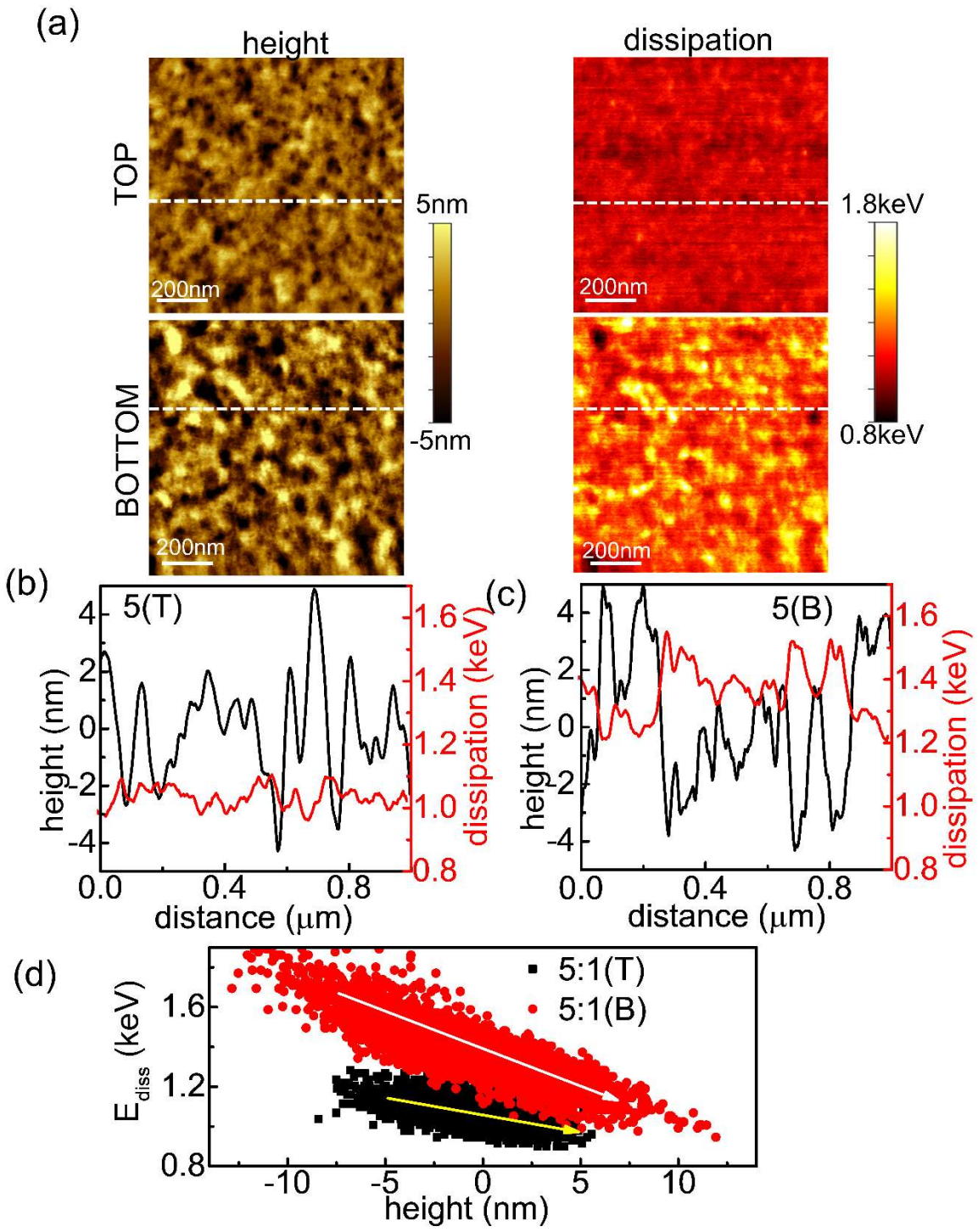

Fig. S8 (a) (left) Topography and (right) energy dissipation for top and bottom side PDMS with 5:1 chemical ratio. Height and energy dissipation profiles over (b) 5(T), and (c) 5(B), along the dashed cross-section lines indicated in Fig. S8(a). (d) The relationship between height and E_{diss}. The x, y-location of each point on the scatterplots corresponds to its height and E_{diiss}. The auxiliary arrows were overlaid to clarify their correlations.

From the scattering plots in Fig. S8(d), we calculated the correlation coefficient, ρ defined as the

following equation:

$$\rho = \frac{\sum_{i=1}^{n}(x_i-\bar{x})(y_i-\bar{y})}{(n-1)s_x s_y} \quad \text{(S6)}$$

In the equation, x_i, and y_i represents the i-th data points. Accordingly, $\bar{\boldsymbol{x}}$ and $\bar{\boldsymbol{y}}$ are their mean values, while s_x and s_y are their stand deviation values. n corresponds to the total pixel number of a SPM image. From the data pixels of Fig. S8(a), while ρ was calculated as ~0.50 for 5(T)-PDMS, the value greatly decreased to –0.86 for 5(B)-PDMS. Such a negative value close to -1, indicates that the P/F-method not only enhances E_{diss} over the entire area, but also reinforces the correlation between height and E_{diss}. The results agree with the line profiles in Fig. S8(b) and (c).

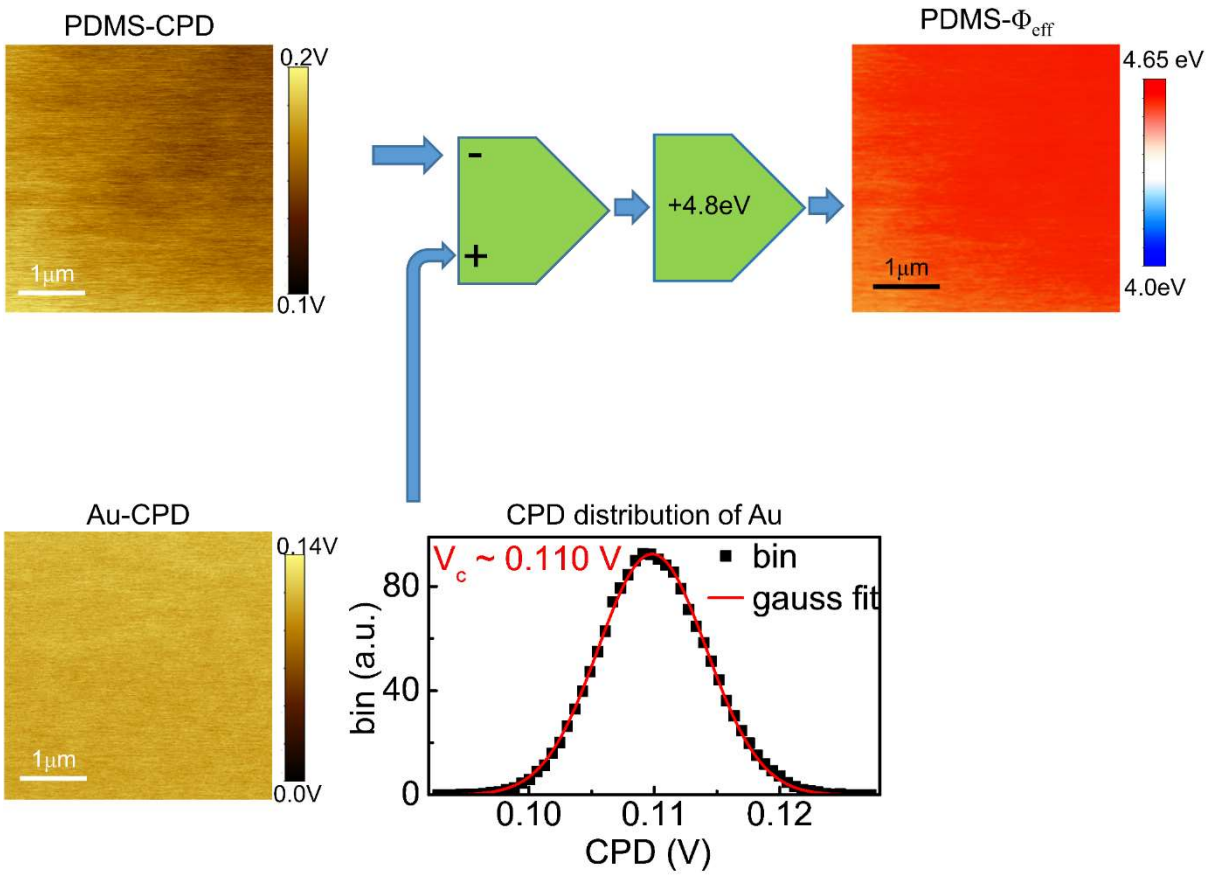

Fig. S9 The conversion process of contact potential difference (CPD) image to work function one, in reference to Au. The work of work function (Φ_{Au}) is assumed to be 4.8 eV.

In a KPFM with tip-bias mode, the measured CPD can be defined as

$$\mathrm{CPD} = \frac{\Phi_{tip} - \Phi_{sample}}{e} \qquad \text{(S6)}$$

where Φ_{tip} and Φ_{sample} denote the work functions of tip and sample, respectively. In this study, instead of characterizing Φ_{tip} separately, Au-pads are locally formed by sputtering on the PDMS surface using a shadow mask. Thus, if CPD over the PDMS region is observed together with a neighboring Au-region, Φ_{sample} can be extracted using the relation:

$$\mathrm{CPD}_{Au} - \mathrm{CPD}_{PDMS} = \frac{(\Phi_{tip} - \Phi_{Au}) - (\Phi_{tip} - \Phi_{PDMS})}{e} \qquad \text{(S7a)}$$

$$\Phi_{PDMS} = e(\mathrm{CPD}_{Au} - \mathrm{CPD}_{PDMS}) + \Phi_{Au} \qquad \text{(S7b)}$$

In this study, we assumed that Φ_{Au} is 4.8 eV. As Φ_{sample} can be readily estimated in the method, regardless of the Φ_{tip}, it is useful for characterizing the surface potential of dielectric sample where tip and sample easily alter each other's states during the scanning procedure.

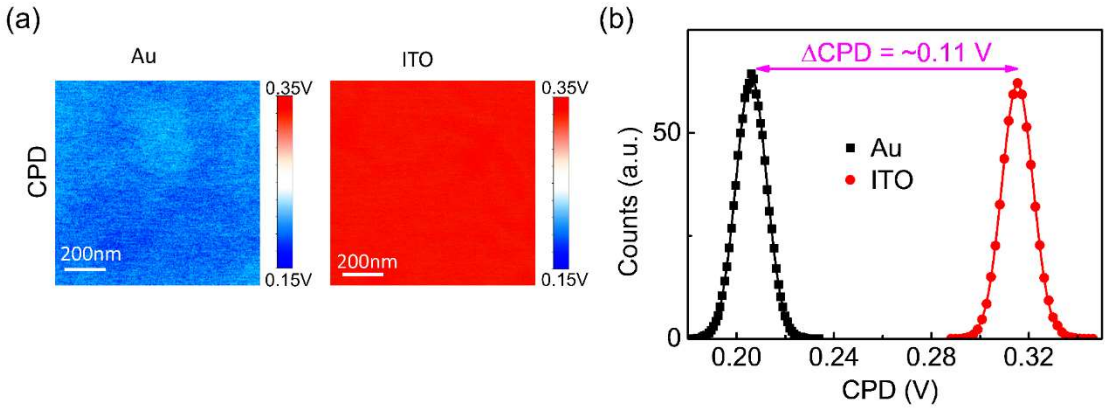

Fig. S10 (a) CPD image obtained on the surface of (left) Au, and (right) ITO films. (b) The corresponding distributions of CPD values (dot). The solids represent Gaussian fitting results used to estimate their work function difference.

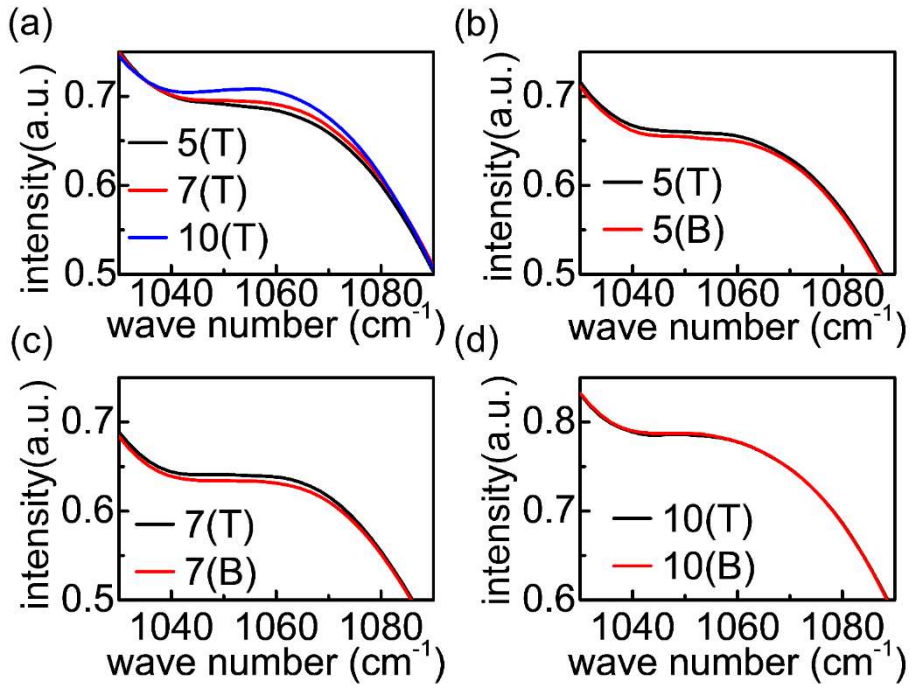

Fig. S11 FTIR spectra of the antisymmetric Si-O-Si stretching mode for six different types of PDMSs

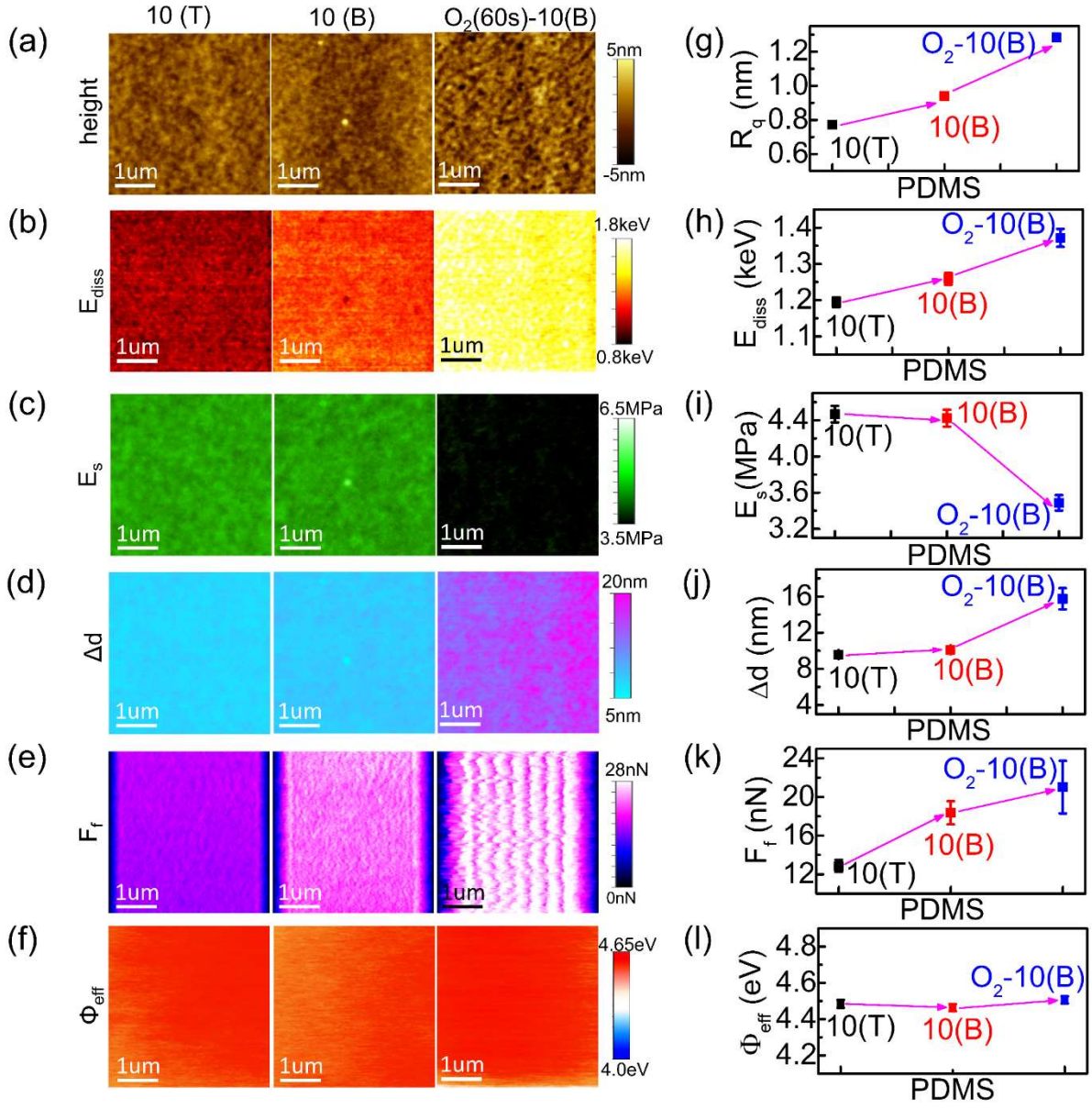

Fig. S12 (a)~(f) Comprehensive SPM image lists for three different 10:1-PDMS ((left) top, (middle) bottom, and (right) 60-sec-O_2-pretreated-bottom): (a) topography, (b) energy dissipation, (c) modulus, (d) deformation, (e) friction, and (f) effective work function images. The images of (a)-(d) are simultaneously obtained from PF-AFM, while LFM and KPFM were employed for (e) and (f), respectively. (g)-(l) The distribution variations corresponding to SPM image contrasts

References

1. H. Wang, S. Huang, H. Kuang, C. Zhang, Y. Liu, K. Zhang, X. Cai, X. Wang, J. Luo and Z. L. Wang, *Advanced Energy Materials*, 2023, **13**, 2300529.
2. J. H. Kim, J. Jeong, D. S. Kong, H. Yoon, H. Cho, J. H. Jung and J. Y. Park, *Advanced Materials Interfaces*, 2024, **11**, 2300821.
3. S. Niu, S. Wang, L. Lin, Y. Liu, Y. S. Zhou, Y. Hu and Z. L. Wang, *Energy & Environmental Science*, 2013, **6**, 3576-3583.
4. R. W. Carpick, D. Ogletree and M. Salmeron, *Applied Physics Letters*, 1997, **70**, 1548-1550.
5. S. Kwon, J.-H. Ko, K.-J. Jeon, Y.-H. Kim and J. Y. Park, *Nano letters*, 2012, **12**, 6043-6048.
6. M. Lantz, S. O'shea, A. Hoole and M. Welland, *Applied physics letters*, 1997, **70**, 970-972.
7. J. C. Lötters, W. Olthuis, P. H. Veltink and P. Bergveld, *Journal of micromechanics and microengineering*, 1997, **7**, 145.
8. B. V. Derjaguin, V. M. Muller and Y. P. Toporov, *Journal of Colloid and interface science*, 1975, **53**, 314-326.
9. J. E. Jakes, *Journal of materials science*, 2018, **53**, 4814-4827.
10. J. D. Musgraves, J. Hu and L. Calvez, *Springer handbook of glass*, Springer, 2019.

